Received February 3, 2020, accepted February 21, 2020, date of publication March 5, 2020, date of current version March 17, 2020.

Digital Object Identifier 10.1109/ACCESS.2020.2978695

Evaluation of Predictive Current Control Techniques for PM BLDC Motor in Stationary Plane

MANISH S. TRIVEDI[1] AND RITESH KUMAR KESHRI[1], (Senior Member, IEEE)
Department of Electrical Engineering, Visvesvaraya National Institute of Technology, Nagpur 440010, India

Corresponding author: Manish S. Trivedi (manish.trivedi@students.vnit.ac.in)

This work was supported by the Ministry of Electronics and Information Technology, Government of India.

ABSTRACT In general, PM BLDC motors are injected with square wave phase currents through PI-PWM control in a-b-c reference plane to ensure maximum torque-per-ampere. The operation of PM BLDC motor in a stationary plane has shown considerable simplification in design, and analysis in the control techniques. The present paper considers the injection of square wave phase current through predictive current control strategies in the stationary plane. For the evaluation of performance, cases of deadbeat predictive control, hysteresis based predictive control, and finite control-set model predictive control (FCS-MPC) methods are considered. Control schemes have been designed for 48V, 660W PM BLDC motor. Comparative evaluation is carried out in terms of the harmonic components available in the current and torque, tracking of the current trajectory in the stationary plane in the low and high-speed region, and execution time of all the control methods. Considered predictive methods are tested on an experimental prototype, and control is implemented through digital Signal Processor (DSP) TMS320F28335. Evaluation leads to the conclusion that predictive control performs better than PI-PWM for reducing commutation torque ripple, keeping current harmonics under control. It is observed that predictive control strategies in the stationary plane, improve the torque-speed characteristic to the wider utilization of constant torque zone of operation as compared to conventional strategies.

INDEX TERMS Current control, PM BLDC motor, predictive control, stationary plane control.

I. INTRODUCTION

Permanent magnet (PM) brushless dc (BLDC) motor, with non-sinusoidal back-EMF waveform, uses rotor position information from hall sensors to inject phase current synchronized with the flat portion of the back-emf [1]. This motor is widely used in home appliances, automotive applications, medical equipment, aerospace, and robots [2]–[4]. The issue of the torque ripple, due to phase current commutation during phase commutation after each 60° of electrical angle, affects the torque-speed performance of the machine and limits the utilization of the constant torque zone of operation. Commutation torque ripple can be up to 50% with respect to the nominal average torque [5]. Other torque ripples such as one due to PWM operation of the inverter can be minimized through proper selection of the switching frequency and whereas torque ripple due to cogging has design limitations. The original analysis of phase commutation for PM BLDC motor is carried out in [6], [7]. In this analysis, the author shows that during phase commutation due to motor phase inductance and limited DC link voltage, incoming and outgoing phase currents have different rise/fall rates at different speeds. This unequal slope rate of incoming and outgoing phase current produces torque ripple in the motor. In general, torque ripple issue is addressed through the equalization of slopes of the incoming or outgoing phase currents as per the lower or higher speed range and realized by the PWM control techniques with appropriate duty ratio control of the respective phase switches of the inverter [8]–[10]. These techniques require information about the commutation duration either by the computation through the employed micro-controller or dedicated hardware circuitry. In [11], the three-segment modulation method for a full-speed range is used for the generation of duty ratio, which is based on complex analytical

The associate editor coordinating the review of this manuscript and approving it for publication was Zhehan Yi.

computation in the three-phase system. In all conventional methods, classical control theory is used to generate the PWM signal by using a linear system model which is highly complex and requires extensive tuning. Also, for operating PM BLDC motor by using the conventional methods, high speed and low-speed cut of points have to be detected precisely. Inappropriate detection results in the degradation of performance.

Torque ripple reduction by using the current control technique is highly effective in case of PM BLDC motor and mostly ensured through the PWM strategy. Whereas predictive control techniques are much effective, simple to understand, intuitive, easy to implement and are mostly classified as deadbeat control, hysteresis based and model predictive control (MPC) as applied to power electronics and drives [12]. Performance of PM BLDC motor with MPC has been evaluated by some of the researchers, whereas other strategies are yet required to be evaluated. Control of PM BLDC motor in the stationary plane as compared to a-b-c frame of reference has advantages of reduced analytical burden and has independent control over commutation torque ripple, commutation time, active/reactive power flow, and it is easy to implement [13], [14]. Model predictive control is applied for PM BLDC motor in a-b-c reference frame in some cases for reduction of commutation torque ripple [15], for improved dynamic behavior [16] and for position control [17]. With the emergence of stationary frame analysis for PM BLDC motor [18], analysis for the control method gets easier. New control techniques applied to PM BLDC motor are in the stationary frame. In [19], improvement in commutation torque ripple and commutation time in the stationary frame, based on the application of voltage vector during commutation, is analyzed for full speed range and depending on the speed with different loading is shown in [13]. Commutation torque ripple reduction in motoring and generating mode based on hysteresis current control in the stationary frame [20] gives ease in the analysis. A simple control structure based on the flux-based controller reduces torque ripple in the stationary frame [21]. Analysis based on stationary frame based model predictive power control for commutation torque ripple reduction is presented in [22], which gives a simple control technique. From the available literature, predictive control applied to PM BLDC motor in the stationary frame is in one case [22]. This control is based on predictive power control. Predictive current control for PM BLDC motor in the stationary frame is not available in the literature and not explored completely. In this paper, all predictive current control methods with analysis in the stationary frame, are being developed and implemented for PM BLDC motor. Predictive current control methods with stationary frame analysis have combined advantages of predictive control as well as a stationary frame of reference. Predictive control method, namely deadbeat control, hysteresis based and model predictive control, has been used in many applications other than PM BLDC motor, which gives better performance in terms of current control, simple in analysis and less complex in implementation as compared to the conventional control method. In [23]–[25] deadbeat predictive current control is being used for PMSM motor, which gives advantages over conventional as simple control, better transient response, less complex computation, and improved accuracy in tracking. In [26]–[28] predictive hysteresis current control is applied to a different application for the fast transient response, easy implementation, and increased control accuracy over conventional control. In [29]–[32] model predictive control applied to VSI for various applications has advantages like the flexibility of easy inclusion of additional control objective in the cost function, simple optimization algorithm, and improved performance in steady-state and transient as compared to a conventional control technique.

A predictive current control technique in the stationary frame is being applied to PM BLDC motor in this paper to have combined advantages of predictive control and stationary reference frame. In place of DC supply, micro-grid can be used, and whole system analysis with predictive current control will have PM BLDC motor as an application for micro-grid [33]. This research work will be helpful for that application. This paper discusses the proposed predictive current control technique in the stationary frame for commutation torque ripple reduction and control for a full-speed range of PM BLDC motor. The objective of this study is:-

- Application of predictive control method in the stationary frame for PM BLDC motor.
- Benchmarking these predictive current control methods with conventional control method for PM BLDC motor.
- Comparison of computational complexity and performance evaluation of predictive control method for torque ripple reduction capability applied to PM BLDC motor
- Implementation of all predictive control method for PM BLDC motor

Paper is organized as: Section II derives PM BLDC motor modelling in the stationary frame and other considerations. Section III demonstrate predictive control and PI-PWM control schemes. Section IV describes the comparison of predictive control schemes and PI-PWM schemes, and Section V concludes the paper.

II. PM BLDC MOTOR DRIVE

A. STATIONARY FRAME MODELLING

The circuital schematic of PM BLDC motor with input voltage source inverter (VSI) having V_d as a input DC supply is shown in Fig. 1. Each phase of motor shown in Fig. 1 represents R_p, L_p, e_p, v_{pn} and i_p as phase resistance, inductance, back-EMF, phase to neutral voltage and phase current for phase $p = a$, b and c. Injected square wave phase current, synchronized with the flat top portion of the trapezoidal back-EMF for ideal PM BLDC motor is shown in Fig. 2.

With the condition of power invariance phase variables, $\boldsymbol{x}$ in a-b-c plane of reference can be transformed into a stationary plane through (1), where $\boldsymbol{x}$ can be phase voltage,

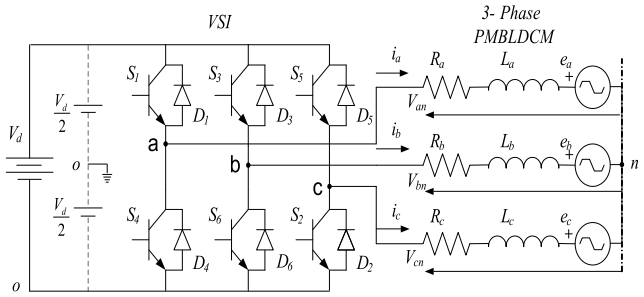

FIGURE 1. Circuital schematic of three phase PM BLDC drive.

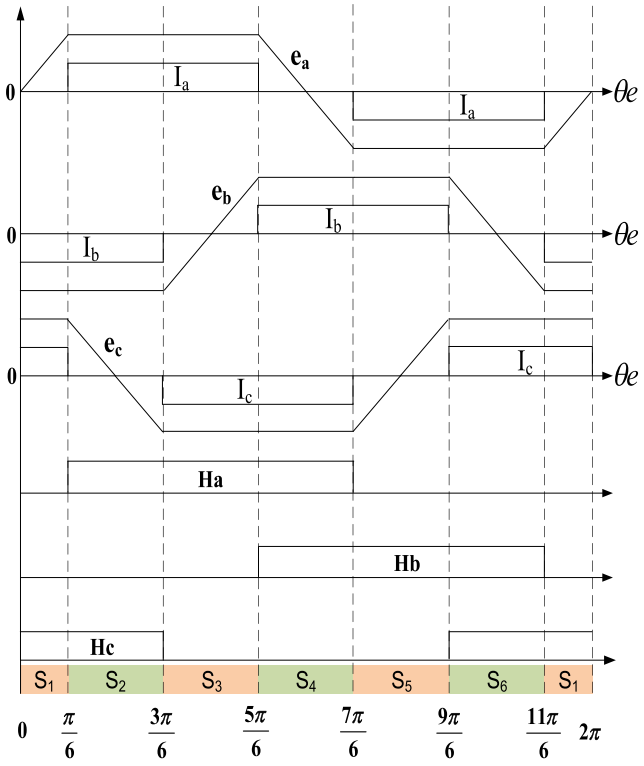

FIGURE 2. Back emf and phase current of PM BLDC motor.

current, and back-EMF. Fig. 2 shows the phase back-EMF and injected phase currents together with the three Hall sensor signals from the PM BLDC motor. Fig.3 shows the transformed current and the back-EMF vectors in six-sectors S_1 to S_6 corresponding to the six-hall states.

$$\begin{bmatrix} x_\alpha \\ x_\beta \end{bmatrix} = \frac{2}{3}\begin{bmatrix} 1 & -\frac{1}{2} & -\frac{1}{2} \\ 0 & \frac{\sqrt{3}}{2} & -\frac{\sqrt{3}}{2} \end{bmatrix}\begin{bmatrix} x_a \\ x_b \\ x_c \end{bmatrix} \tag{1}$$

The electrical dynamic equation for PM BLDC motor is transformed into a stationary frame using (1) is given by (2).

$$\frac{d}{dt}\begin{bmatrix} i_\alpha \\ i_\beta \end{bmatrix} = \begin{bmatrix} -\frac{R}{L} & 0 \\ 0 & -\frac{R}{L} \end{bmatrix}\begin{bmatrix} i_\alpha \\ i_\beta \end{bmatrix} + \begin{bmatrix} \frac{1}{L} & 0 \\ 0 & \frac{1}{L} \end{bmatrix}\begin{bmatrix} v_\alpha - e_\alpha \\ v_\beta - e_\beta \end{bmatrix} \tag{2}$$

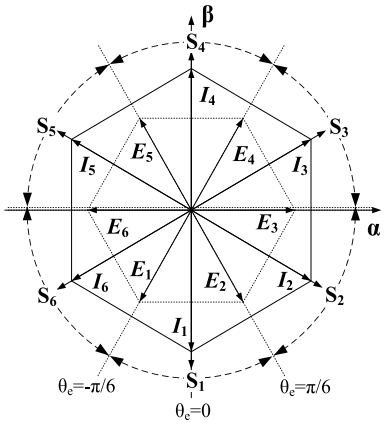

FIGURE 3. Trajectories of back-EMF and current vectors.

TABLE 1. $\alpha - \beta$ co-ordinate of current and back-EMF.

$i; e$	$(I_\alpha, I_\beta); (E_\alpha, E_\beta)$
$I_1; E_1$	$(0, -\frac{2}{\sqrt{3}})I; (-\frac{2}{3}, -\frac{2}{\sqrt{3}})E$
$I_2; E_2$	$(1, -\frac{1}{\sqrt{3}})I; (\frac{2}{3}, -\frac{2}{\sqrt{3}})E$
$I_3; E_3$	$(1, \frac{1}{\sqrt{3}})I; (\frac{4}{3})E$
$I_4; E_4$	$(0, \frac{2}{\sqrt{3}})I; (\frac{2}{3}, \frac{2}{\sqrt{3}})E$
$I_5; E_5$	$(-1, \frac{1}{\sqrt{3}})I; (-\frac{2}{3}, \frac{2}{\sqrt{3}})E$
$I_6; E_6$	$(-1, -\frac{1}{\sqrt{3}})I; -(\frac{4}{3})E$

The phase-vectors $\boldsymbol{v} = v_\alpha + jv_\beta$ and $\boldsymbol{e} = e_\alpha + je_\beta$ are represented in terms of a-b-c plane of the reference phase variables by (3) and (4).

$$\boldsymbol{v} = \begin{bmatrix} v_\alpha \\ v_\beta \end{bmatrix} = \begin{bmatrix} \frac{2}{3}v_{ao} - \frac{v_{bo}}{3} - \frac{v_{co}}{3} \\ \frac{1}{\sqrt{3}}(v_{bo} - v_{co}) \end{bmatrix} \tag{3}$$

$$\boldsymbol{e} = \begin{bmatrix} e_\alpha \\ e_\beta \end{bmatrix} = \begin{bmatrix} \frac{2}{3}e_a - \frac{e_b}{3} - \frac{e_c}{3} \\ \frac{1}{\sqrt{3}}(e_b - e_c) \end{bmatrix} \tag{4}$$

where, $v_{po}(p = a, b, c)$ is the motor terminal voltage measured with respect to the virtual mid-point "o" of the dc-link voltage V_d. The transformed back-EMF waveform in the stationary frame, as shown in Fig. 3 is defined for each phase in a-b-c reference frame as given in (5) and transformed using (4). In (5), $E = k_b w_m$ is the amplitude of back-EMF in which rotor angular speed is represented by w_m, and k_b represents back-EMF constant. The stationary frame co-ordinates for current and back-EMF is shown in Table. 1.

$$e = s(1 - \frac{6}{\pi}(\theta_e - \theta_s))E \tag{5}$$

whereas in (5), θ_e and θ_s are the electrical angle and the angle at the starting of the transition, respectively, and s is 1 when the transition is from E to $-$E and -1 when the transition is from $-$E to E.

The active electrical power converted into mechanical power for the generation of electromagnetic torque is given

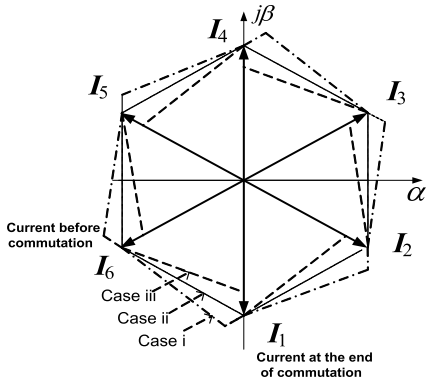

FIGURE 4. Current vector trajectory at different speed.

TABLE 2. Voltage vector table.

Sector	Angle	Voltage vector during commutation	Voltage vector during non-commutation
S_1	$(11\pi/6)-(\pi/6)$	$\boldsymbol{V}_2 = (\frac{1}{3} - j\frac{1}{\sqrt{3}})V_d$	$\boldsymbol{V}_{12} = (0 - j\frac{1}{\sqrt{3}})V_d$
S_2	$(\pi/6)-(3\pi/6)$	$\boldsymbol{V}_3 = \frac{2}{3}V_d$	$\boldsymbol{V}_{23} = (\frac{1}{2} - j\frac{1}{2\sqrt{3}})V_d$
S_3	$(3\pi/6)-(5\pi/6)$	$\boldsymbol{V}_4 = (\frac{1}{3} + j\frac{1}{\sqrt{3}})V_d$	$\boldsymbol{V}_{34} = (\frac{1}{2} + j\frac{1}{2\sqrt{3}})V_d$
S_4	$(5\pi/6)-(7\pi/6)$	$\boldsymbol{V}_5 = (-\frac{1}{3} + j\frac{1}{\sqrt{3}})V_d$	$\boldsymbol{V}_{45} = (0 + j\frac{1}{\sqrt{3}})V_d$
S_5	$(7\pi/6)-(9\pi/6)$	$\boldsymbol{V}_6 = -\frac{2}{3}V_d$	$\boldsymbol{V}_{56} = (-\frac{1}{2} + j\frac{1}{2\sqrt{3}})V_d$
S_6	$(9\pi/6)-(11\pi/6)$	$\boldsymbol{V}_1 = (-\frac{1}{3} - j\frac{1}{\sqrt{3}})V_d$	$\boldsymbol{V}_{61} = (-\frac{1}{2} - j\frac{1}{2\sqrt{3}})V_d$

by (6)

$$T_e = \frac{P}{\omega_m} = \frac{i_\alpha e_\alpha + i_\beta e_\beta}{\omega_m} \tag{6}$$

Due to motor inductances and limited DC voltage supply, the current trajectory shown in Fig. 3 will not take instantaneous transition and, in practice, will transit as shown in Fig. 4, causing ripples in motor torque.

B. VOLTAGE SELECTION

In PM BLDC motor operation, two phases and three phases get involve during non-commutation and commutation duration, respectively. For selecting an appropriate vector during PM BLDC motor operation, commutation duration has to be identified. Commutation duration is calculated with the method shown in [15] in which the starting moment of commutation is detected based on hall sensor rise or fall, and the end of commutation depends on the zero-phase current of that sector. No extra circuit is required for the detection of commutation duration in this method. The vector table for commutation and non-commutation duration depending on the sector of operation is shown in Table. 2, and the corresponding vector diagram is shown in Fig. 5. Three-phase and two-phase modulating vectors are being selected according to commutation duration.

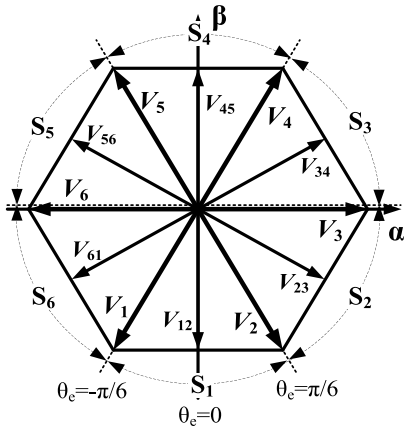

FIGURE 5. Commutation and non-commutation voltage vector diagram.

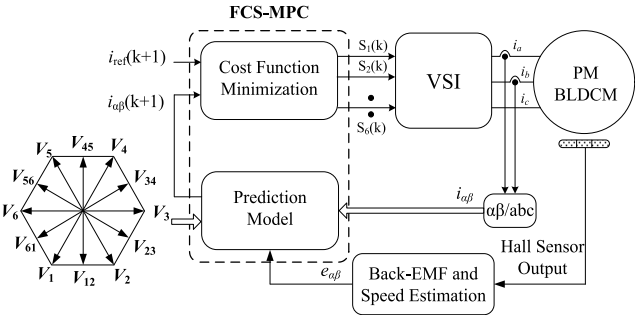

FIGURE 6. Block diagram of model predictive control for PM BLDC motor.

III. PREDICTIVE CURRENT CONTROL AND PI-PWM CONTROL SCHEMES

The principle of operation of all predictive control techniques is explained first, and then its complexity in implementation is discussed. Next, PI-PWM control is considered for comparison.

A. FINITE CONTROL-SET MODEL PREDICTIVE CONTROL (FCS-MPC)

As described in [15], FCS-MPC in the natural reference frame (a-b-c frame) is being used for PM BLDC motor for commutation torque ripple reduction. Stationary frame representation [18] of PM BLDC motor helps to get a predictive model in the stationary plane. The block diagram of FCS-MPC for PM BLDC motor is shown in Fig. 6. In this block diagram, a predictive model is derived from the discretized model of (2) given in (7).

$$\boldsymbol{i}(k+1) = (1 - \frac{R}{L}T_s)\boldsymbol{i}(k) + \frac{T_s}{L}\boldsymbol{v}(k) - \frac{T_s}{L}\boldsymbol{e}(k) \tag{7}$$

Model (7) is derived from (2) with the approximation

$$\frac{d\boldsymbol{i}}{dt} = \frac{\boldsymbol{i}(k+1) - \boldsymbol{i}(k)}{T_s} \tag{8}$$

where T_s is a sampling time. The estimation of motor back-EMF derived from (7) as given in (9)

$$\boldsymbol{e}(k) = \boldsymbol{v}(k) - \frac{L}{T_s}\boldsymbol{i}(k+1) + R(\frac{L}{RT_s} - 1)\boldsymbol{i}(k) \tag{9}$$

for small sampling interval $\boldsymbol{e}(k+1) = \boldsymbol{e}(k)$. The predicted value of feedback current for all available voltage vectors depending on the duration as commutation or non-commutation Table. 2 can be estimated from (7). The voltage vector, which gives minimum error in current prediction from the reference current, is applied in the next sampling instant. The cost function representing this is given by (10).

$$g = (\boldsymbol{i}_{ref} - \boldsymbol{i}(k+1))^2 \tag{10}$$

The strategy for MPC control:-

- The reference current $\boldsymbol{i}_{ref}$ is generated and transformed into a stationary frame with the help of hall sensor position and speed of the motor as in Fig. 2 and Fig. 3.
- For getting the predictive model, the feedback current and back-EMF are transformed into stationary frame.
- For all the voltage vector, feedback current is predicted for the next sampling instant using present feedback current and estimated back-EMF for commutation and non-commutation duration.
- Cost function g for all predicted current is estimated depending on the duration of the operation.
- The voltage vector, which gives the minimum value of cost function g, is applied in the next switching instant.

In case of PM BLDC motor, current trajectory in Fig. 4 deviates from ideal mode (case ii) during low speed (case i) and high speed (case iii) due to the inductance of the motor phases during incoming and outgoing phase current since it takes finite time for current to rise and fall. The advantage of FCS-MPC control is that it works for the full speed range without differentiating high speed and low-speed operation. It applies control in every sampling instant to track the ideal mode current (case ii) in Fig. 4 using the predictive model in (7). The control effectively reduces commutation torque ripple compared to the conventional method.

B. PREDICTIVE DEADBEAT CURRENT CONTROL (PDCC)

In FCS-MPC, the cost function is used as a switching logic for PM BLDC motor operation. The method PDCC uses a space vector modulator (SVM) as a switching logic. The application of deadbeat logic is possible due to the emergence of stationary plane representation of PM BLDC motor. The block diagram for PDCC is shown in Fig. 7.

In this block diagram, the predictive model for getting the reference voltage vector uses the discretize equation in (7). The equation for reference voltage vector $\boldsymbol{v}(k)$ is given in (11),

$$\boldsymbol{v}(k) = \frac{L}{T_s}(\boldsymbol{i}_{ref}(k) - \boldsymbol{i}(k+1)) + R\boldsymbol{i}(k+1) + \boldsymbol{e}(k+1) \tag{11}$$

the reference voltage vector $\boldsymbol{v}(k)$ is the present voltage vector. The desired reference voltage vector to achieve $\boldsymbol{i}(k+2)$

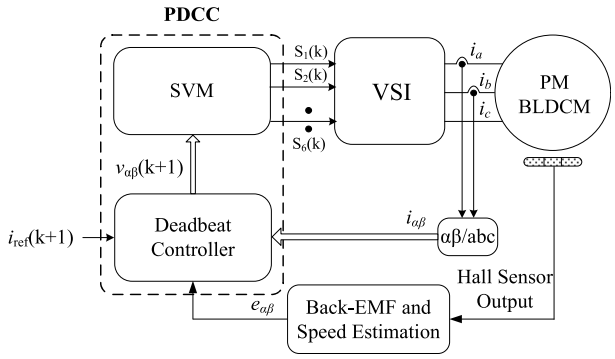

FIGURE 7. Block diagram of predictive deadbeat current control for PM BLDC motor.

current vector given in (12) is $\boldsymbol{v}(k+1)$ (13). It will give accurate reference tracking for PM BLDC motor.

$$\boldsymbol{i}(k+2) = (1 - \frac{R}{L}T_s)\boldsymbol{i}(k+1) + \frac{T_s}{L}\boldsymbol{v}(k+1) - \frac{T_s}{L}\boldsymbol{e}(k+1) \tag{12}$$

$$\boldsymbol{v}(k+1) = \frac{L}{T_s}(\boldsymbol{i}_{ref}(k) - \boldsymbol{i}(k+2)) + R\boldsymbol{i}(k+2) + \boldsymbol{e}(k+2) \tag{13}$$

In this case, back-EMF vector $\boldsymbol{e}(k)$ and $\boldsymbol{e}(k+1)$ is assumed to be constant for one sampling instant. Tracking the trajectory in case (ii) Fig. 4, the reference voltage vector $\boldsymbol{v}(k+1)$ has to be obtained from available voltage vectors. The SVM modulator is being used to get the desired reference voltage vector in (13). The vector applied for SVM is shown in Table. 2 according to the duration as commutation or non-commutation.

For obtaining the reference voltage vector, the SVM technique is used, which depends on "volt-second balance" as in (14)

$$\boldsymbol{v}_s(k+1)T_s = \boldsymbol{V}_1 t_a + \boldsymbol{V}_2 t_b + \boldsymbol{V}_0 t_0 \tag{14}$$

where T_s is sampling time, which is equal to $t_a + t_b + t_0$ and t_a, t_b, t_0 are the time duration of voltage vectors. Here (14) is used for commutation duration, and (15) is used for non-commutation duration.

$$\boldsymbol{v}_s(k+1)T_s = \boldsymbol{V}_{12} t_a + \boldsymbol{V}_{23} t_b + \boldsymbol{V}_0 t_0 \tag{15}$$

The generalized equation for time duration t_a, t_b, t_0 is given in (16) (ref. chapter 3 [34])

$$\begin{aligned} t_a &= \frac{\sqrt{3}\boldsymbol{v}_s(k+1)}{V_{dc}} sin(N\frac{\pi}{3} - \alpha)T_s \\ t_b &= \frac{\sqrt{3}\boldsymbol{v}_s(k+1)}{V_{dc}} sin(\alpha - (N-1)\frac{\pi}{3})T_s \\ t_0 &= T_s - t_a - t_b \end{aligned} \tag{16}$$

where N is the sector number, and α is the angular displacement of reference voltage vector. Depending on the sector of the reference voltage vector, the adjacent vector is being selected for the application.

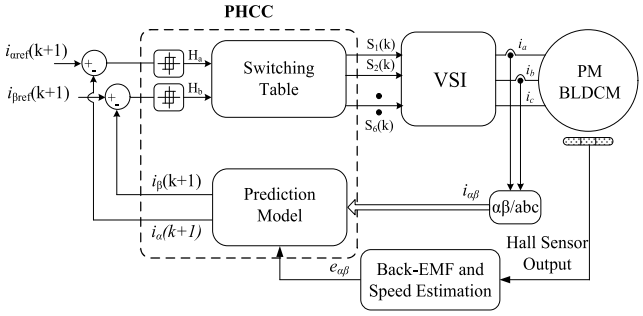

FIGURE 8. Block diagram of predictive hysteresis current control for PM BLDC motor.

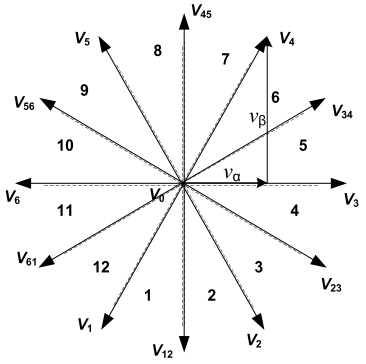

FIGURE 9. Voltage vector plane divided into 12 sectors.

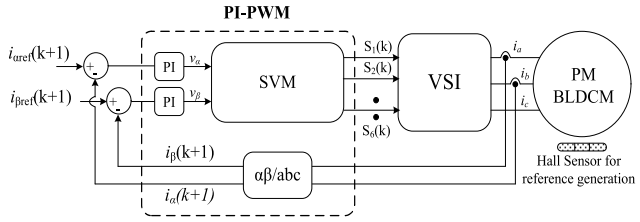

FIGURE 10. Block diagram of PI-PWM current control for PM BLDC motor.

Due to modulator, complexity increases in the implementation, but with that switching frequency gets reduced. It gives more precise control for torque ripple reduction. This technique also works for the whole speed range.

C. PREDICTIVE HYSTERESIS CURRENT CONTROL (PHCC)

Predictive control has one method as predictive hysteresis control in the literature. This method is applied to some applications like static compensator [28], which gives great simplicity and improved results in control. In the case of PM BLDC motor application, hysteresis control is discussed in the natural reference frame. Application of predictive hysteresis control in the stationary frame is not available in the literature, and since it gives increased accuracy in tracking and simplified switching table, this method is applied to PM BLDC motor in this paper.

Since the commutation and non-commutation region, the application of predictive hysteresis control for PM BLDC motor is somewhat different than conventional examples. The block diagram for PHCC is shown in Fig. 8. In this method predictive model is developed using (7). In this equation,

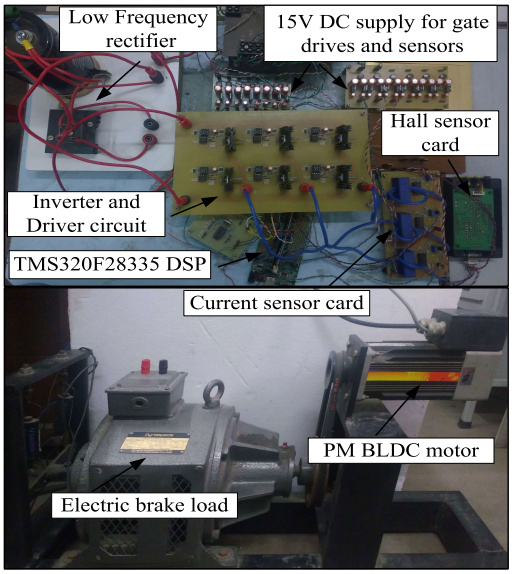

FIGURE 11. Experimental setup for PM BLDC motor control.

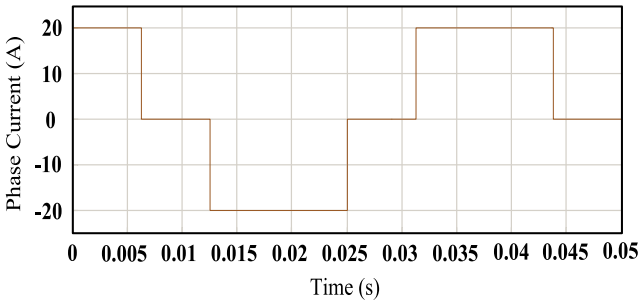

FIGURE 12. Ideal reference current waveform.

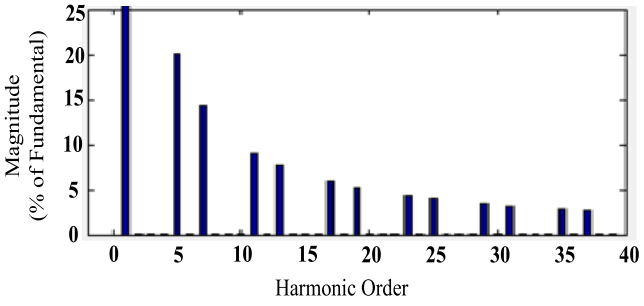

FIGURE 13. Ideal reference current harmonic content.

the equation for back-EMF $\boldsymbol{e}(k)$ is estimated from (9), and for $\boldsymbol{v}(k)$ in (7) for the first iteration, it is considered as zero and for subsequent estimation (17) is being used for determining voltage value.

$$\boldsymbol{v}(k) = \frac{L}{T_s}(\boldsymbol{i}_{ref}(k) - \boldsymbol{i}(k+1)) + R\boldsymbol{i}(k+1) + \boldsymbol{e}(k+1) \quad (17)$$

In this control technique, two hysteresis band is used instead of three hysteresis band. Since stationary plane control is being applied, independent α-axis and β-axis control are possible.

The current control strategy applied for the control with hysteresis band on α and β-axis component, which is having

TABLE 3. Switching table for PHCC.

Hysteresis band		Sector Number											
Ha	Hb	θ_1	θ_2	θ_3	θ_4	θ_5	θ_6	θ_7	θ_8	θ_9	θ_{10}	θ_{11}	θ_{12}
1	1	V_2/V_{12}	V_2/V_{23}	V_3/V_{23}	V_3/V_{34}	V_4/V_{34}	V_4/V_{45}	V_5/V_{45}	V_5/V_{56}	V_6/V_{56}	V_6/V_{61}	V_1/V_{61}	V_1/V_{12}
1	0	V_1/V_{61}	V_1/V_{12}	V_2/V_{12}	V_2/V_{23}	V_3/V_{23}	V_3/V_{34}	V_4/V_{34}	V_4/V_{45}	V_5/V_{45}	V_5/V_{56}	V_6/V_{56}	V_6/V_{61}
0	1	V_2/V_{12}	V_2/V_{23}	V_3/V_{23}	V_3/V_{34}	V_4/V_{34}	V_4/V_{45}	V_5/V_{45}	V_5/V_{56}	V_6/V_{56}	V_6/V_{61}	V_1/V_{61}	V_1/V_{12}
0	0	V_0/V_0	V_0/V_0	V_0/V_0	V_0/V_0	V_0/V_0	V_0/V_0	V_0/V_0	V_0/V_0	V_0/V_0	V_0/V_0	V_0/V_0	V_0/V_0

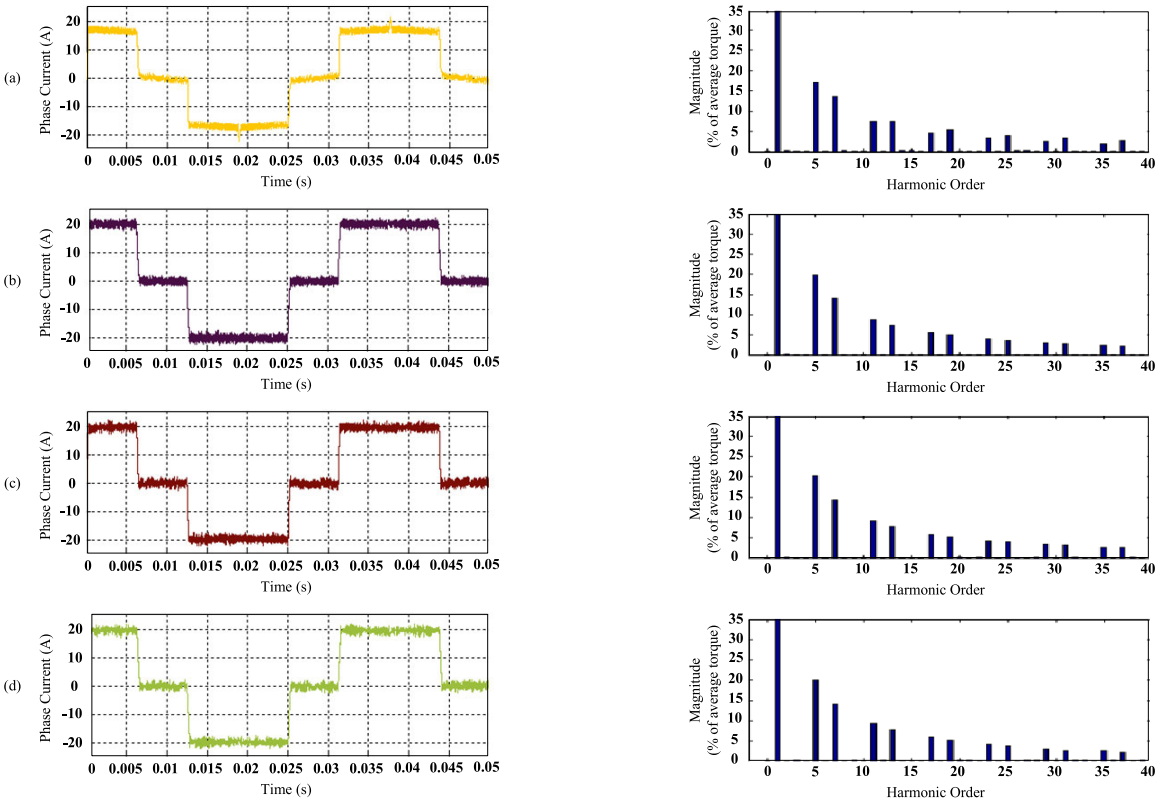

FIGURE 14. Experimental result of stator phase current at low speed of (a) FCS-MPC control; (b) PDCC control; (c) PHCC control (d) PI-PWM control.

output Ha as 1 or 0 and for Hb as 1 or 0. According to these outputs, if Ha is 1, then v_α has to increase, and if Ha is 0, then it has to decrease or remain the same according to the sector of application. For Hb also if Hb is 1, then v_β has to increase, and if Hb is 0, then it has to decrease or remain the same according to the sector of application.

Control strategy for sector 1:-

- *case i*:- Ha $=$ 1 and Hb $=$ 1, both the component are positive means vector, which gives a positive increment in both components in that sector is selected. For commutation duration, $\boldsymbol{V}_2$ is being selected, and for non-commutation duration, $\boldsymbol{V}_{12}$ is being selected according to the above logic.
- *case ii*:- Ha $=$ 1 and Hb $=$ 0, α component has to increase, and β has to maintain or decrease. The vector suitable for this during commutation is $\boldsymbol{V}_1$ and for non-commutation duration $\boldsymbol{V}_{61}$.
- *case iii*:- Ha $=$ 0 and Hb $=$ 1, α component has to be maintained or decreased, and β component has to increase. The vector suitable for this in sector 1 is for commutation duration $\boldsymbol{V}_2$ and non-commutation duration $\boldsymbol{V}_{12}$.
- *case iv*:- Ha $=$ 0 and Hb $=$ 0, both the component have to be maintained or decreased. The vector suitable for this during commutation and non-commutation interval is $\boldsymbol{V}_0$.

Due to the application of the switching table, the switching frequency can be controlled, and with the predicted model, the required switching in the next sampling interval is achieved. The switching table for the PHCC control technique is shown in Table. 3. The sector division and vector available during commutation and non-commutation duration is shown in Fig. 9 where vector for commutation and non-commutation are same as in Fig. 5 and Table. 2.

D. PI-PWM CONTROL

The conventional PI-PWM control, as in [9] and [18] for PM BLDC motor, is applied in this paper for comparison with predictive control methods. The block diagram for control of the PI-PWM control technique is shown in Fig. 10.

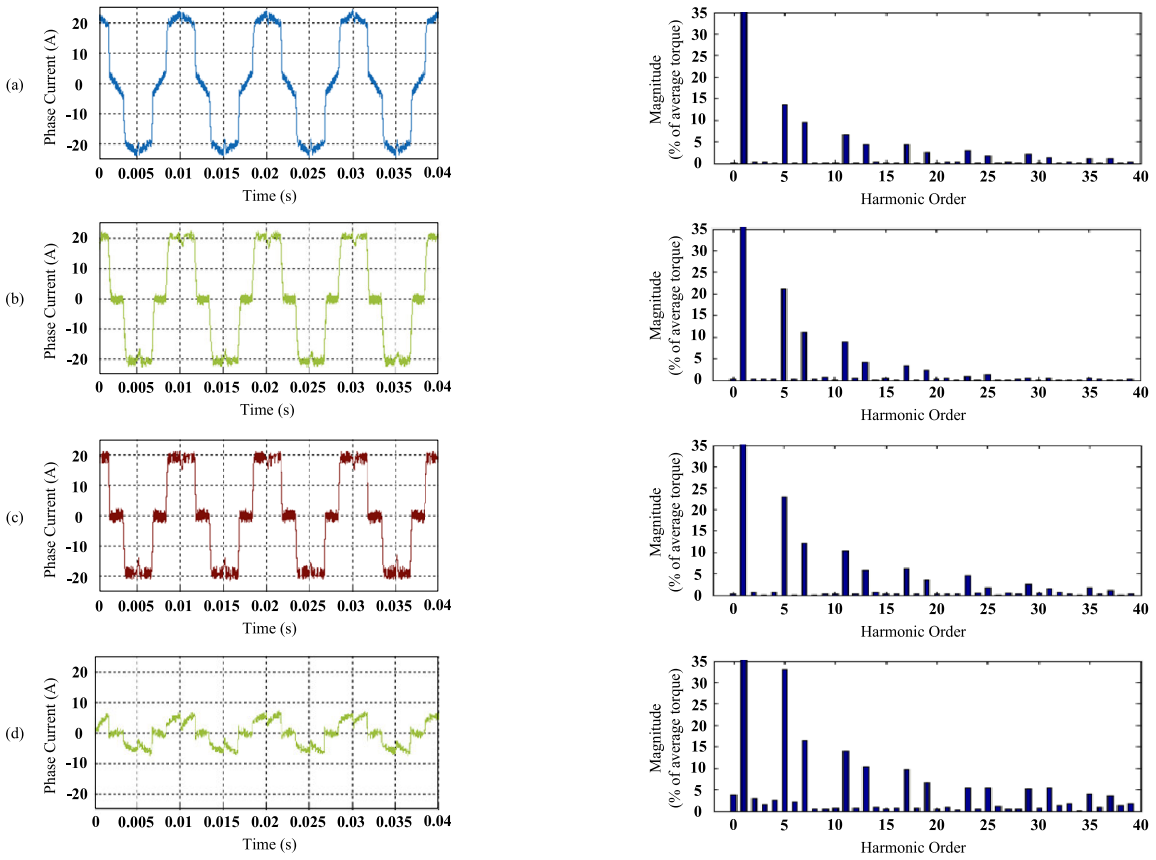

FIGURE 15. Experimental result of stator phase current at high speed of (a) FCS-MPC control; (b) PDCC control; (c) PHCC control (d) PI-PWM control.

The control is implemented in a stationary plane with the tuning of PI parameters. The generation of switching for VSI is achieved using the SVM technique since control is in the stationary frame. The application of the SVM technique (15) and (16) is used in this method. Selection of vectors depending on the duration of operation as commutation or non-commutation is according to Table. 2.

IV. COMPARISON OF PREDICTIVE CONTROL AND PI-PWM SCHEMES

Experimentation is carried out for the predictive current control method and PI-PWM on the setup shown in Fig. 11. In this setup, PM BLDC motor with parameter in Table. 4 is coupled with a brake load of rating 1 kW. The PM BLDC motor is having three hall sensors for position and speed sensing in control operation. The block diagram shown in each predictive control method is implemented on a 32-bit floating point processor DSP TMS320F28335 with information for position and speed is provided to 12-bit ADC by hall sensor card having op-amp IC TL064. The two phases' current signal and DC line voltage signal is measured by using LA 55-P current and LV 25-P voltage sensor, respectively, and the output of the current and voltage sensor is processed by op-amp TL064 so that it should not cross 0-3.3 V range of DSP. The applied techniques in DSP give switching pulse in output, which is given for signal conditioning to buffer circuit SN 74LS07N. This conditioned signal is fed to opto-coupler IC 6N137 for isolation between the power and control circuit. The output of opto-coupler is fed to the driver IC MIC4425ZN to drive the MOSFET IRFB4310ZPbF used in three-phase two leg inverter circuit. The 48 V input to the inverter is provided through a low-frequency rectifier with an output of the rectifier is filtered by 4700 μF electrolytic capacitor. The sampling of the signal for control of all the methods is set to 50 μs which gives a constant sampling frequency of 20 kHz.

TABLE 4. Machine parameter.

Symbol	Description	Value
n_p	Number of pole pairs	4
L	Inclusive phase inductance	0.22 mH
R	Phase resistance	0.135 Ω
T_{rated}	Rated torque	3.3 Nm
w_{rated}	Rated speed	2000 rpm
I_N	Rated motor current	20 A
V_N	Rated motor voltage	48 V
k_b	back-EMF constant	0.1648 $V.s/rad$

A. INVESTIGATION OF CURRENT AND TORQUE HARMONICS

Fig. 14 and Fig. 15 shows the actual phase current in the PM BLDC motor phases at the motor speed of 400 rpm at

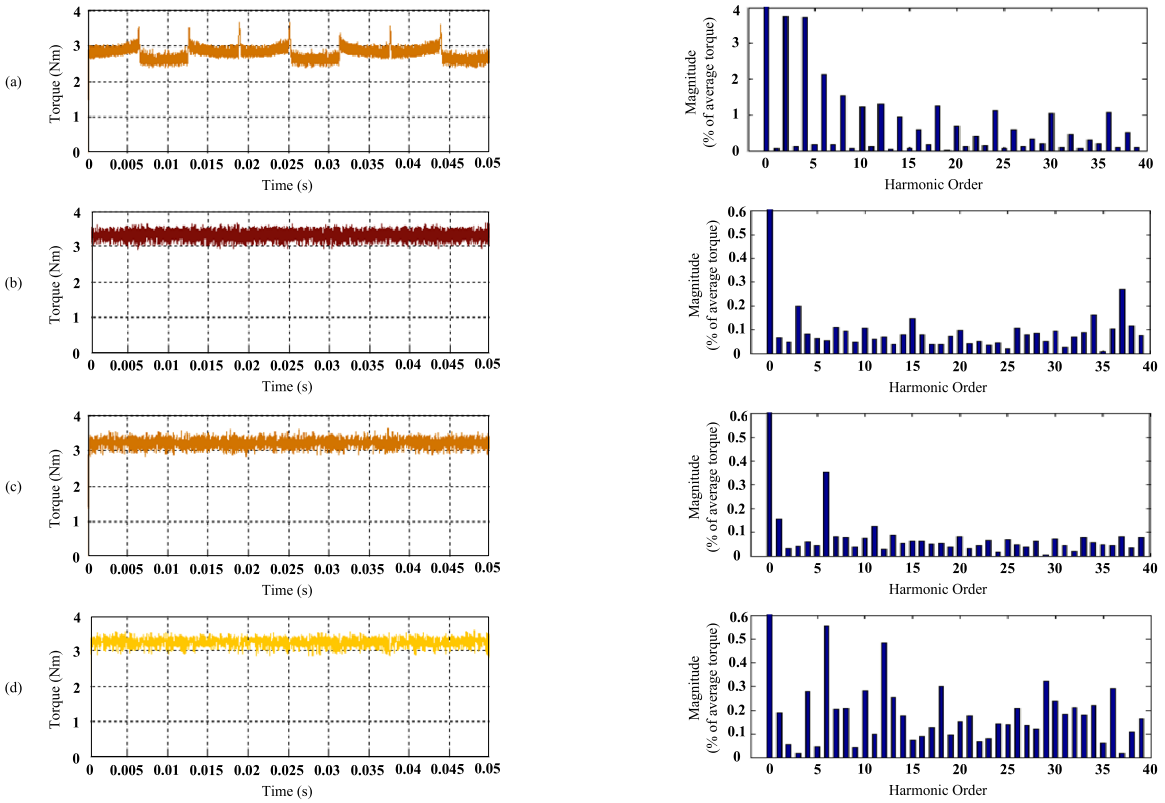

FIGURE 16. Experimental result of torque at low speed of (a) FCS-MPC control; (b) PDCC control; (c) PHCC control (d) PI-PWM control.

3.3 *Nm* torque, i.e., at low speed and 1500 *rpm* at 3.3 *Nm* torque at high speed, respectively. The ideal quasi-square wave reference current generated for operating PM BLDC motor is shown in Fig. 12 having harmonic content, as shown in Fig. 13. Due to the square wave nature of the phase current, odd harmonics are predominant in the waveform. If the waveform tries to achieve the sinusoidal shape, its low order harmonic automatically reduces due to such shape of the waveform. In Fig. 14(a) FCS-MPC control tries to follow the nature of back-EMF, which is somewhat sine shape. Due to this effect 5^{th} and 7^{th} harmonic component reduces as shown in harmonic analysis. The intended trajectory is the ideal current waveform from which it tries to deviate causing, loose bound control. Fig. 14(b), (c), and (d) show PDCC, PHCC, and PI-PWM current control technique, which maintains the same harmonic content shown in ideal reference current waveform harmonic content in Fig. 13 at low-speed operation. During low-speed, all current control techniques try to maintain the ideal nature of the waveform except FCS-MPC, which deviates from the intended nature. In Fig. 15 during high-speed operation FCS-MPC reduces low order harmonic content of the current waveform due to the sine nature of the waveform, but it does not follow the intended control accurately, as shown in Fig. 15(a). In Fig 15(b) and (c), PDCC and PHCC control work excellently, giving required harmonic content as the ideal one with Fig. 15(c), PHCC control shows somewhat more harmonic content then Fig. 15(b). In Fig. 15(d) PI-PWM control unable to maintain the reference magnitude of control during high speed with increased harmonic content in the current waveform. It shows that PI-PWM control does not work properly during high speed.

Fig. 16 and Fig. 17 shows the steady-state torque waveform during low speed and high speed, respectively, for predictive control and PI-PWM control. The torque waveform contains a predominantly 6^{th} and 12^{th} harmonic component due to the phase commutation of PM BLDC motor during each 60° operation. In Fig. 16(a) the torque waveform is shown by FCS-MPC control, unable to maintain the rated torque of 3.3 *Nm*. The harmonic content of FCS-MPC control shows higher content of 6^{th} and 12^{th} harmonic components with that other harmonic component is also predominant. Fig. 16(d) shows a torque waveform of PI-PWM control, which gives more 6^{th} and 12^{th} harmonic components then PDCC and PHCC in Fig. 16(b) and Fig. 16(c), respectively, but lesser than FCS-MPC control. Fig. 16(b) shows PDCC control having the lowest 6^{th} and 12^{th} harmonic components as compared to all other control methods giving the best result during low-speed operation. In Fig. 17(a) FCS-MPC control having less harmonic content then all other control during high speed, but it does not achieve intended 3.3 *Nm* torque. In Fig. 17(b) PDCC control and Fig. 17(c) PHCC control shows the same 6^{th} and 12^{th} harmonic component magnitude with respect to average torque. In Fig. 17(d) PI-PWM control

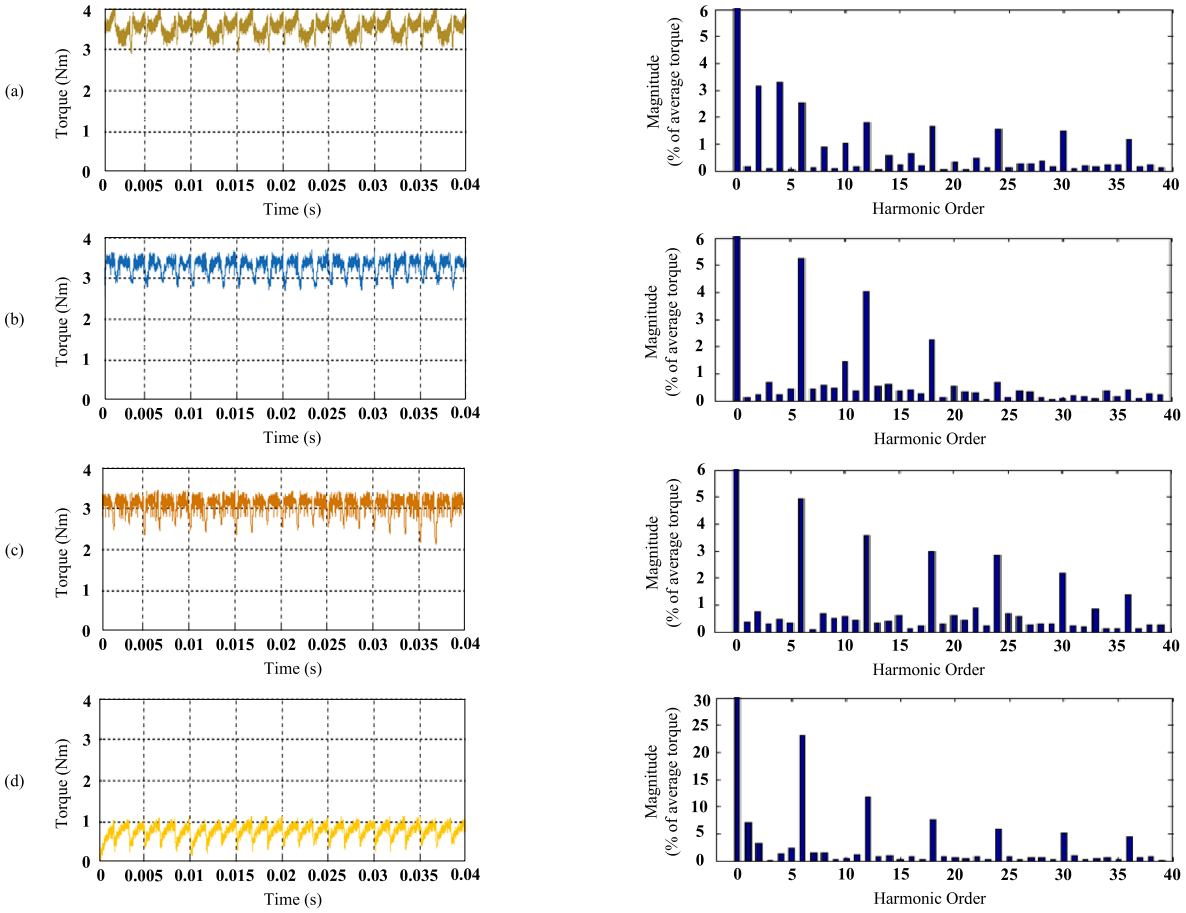

FIGURE 17. Experimental result of torque at high speed of (a) FCS-MPC control; (b) PDCC control; (c) PHCC control (d) PI-PWM control.

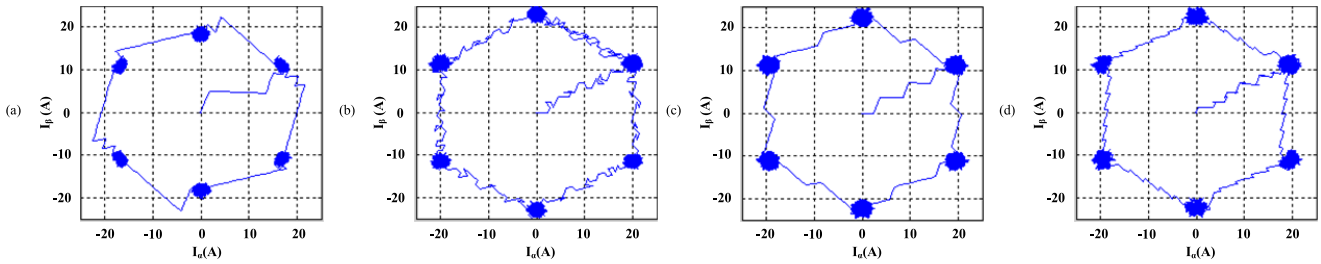

FIGURE 18. Experimental result of stationary current at low speed of (a) FCS-MPC control; (b) PDCC control; (c) PHCC control (d) PI-PWM control.

fails during high speed and shows a high amount of 6^{th} and 12^{th} harmonic component. The 6^{th} and 12^{th} harmonic component of the torque waveform during low-speed and high-speed operation shows that the PDCC control gives the best performance for PM BLDC motor operation.

Fig. 18 and Fig. 19 shows a stationary current waveform of predictive control and PI-PWM control for low-speed and high-speed operation, respectively. Fig. 4 shows the trajectory during high-speed and low-speed operation in which we have to achieve an ideal trajectory by proper control. In Fig. 18(b) for low-speed operation and also during high-speed Fig. 19(b) PDCC control works most precisely, as seen by the stationary plane trajectory. FCS-MPC and PHCC control trajectory deviates from ideal nature, as shown in Fig. 18(a) and (c) and Fig. 19(a) and (c), respectively. The PI-PWM control works properly during low-speed, but for high-speed, it is unable to achieve the desired current as shown in Fig. 18(d) and Fig. 19(d), respectively.

B. EXECUTION TIME ANALYSIS

The sampling time for all the methods is kept constant as 50 μs. Table. 5 shows the comparison of the computation time (T_c), free time (T_f), sampling time (T_s), switching frequency (f_{sw}) for all the methods in the paper. Computational

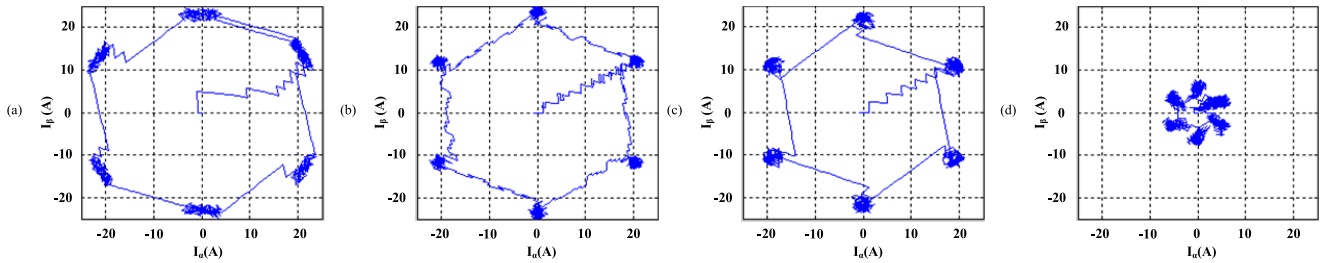

FIGURE 19. Experimental result of stationary current at high speed of (a) FCS-MPC control; (b) PDCC control; (c) PHCC control (d) PI-PWM control.

TABLE 5. Execution time of control algorithm.

Paramteres	PI-PWM	FCS-MPC	PDCC	PHCC
T_s	50 μs	50 μs	50 μs	50 μs
T_C	35 μs	30 μs	36 μs	33 μs
T_f	15 μs	20 μs	14 μs	17 μs
f_{sw}	14 kHz	11.11 kHz	9.25 kHz	10.10kHz

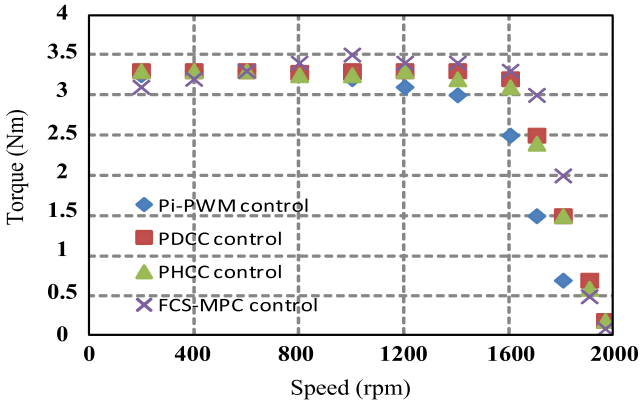

FIGURE 20. Experimental torque-speed characteristic with (cross) FCS-MPC, (square) PDCC, (triangle) PHCC, (diamond) PI-PWM control.

complexity is analyzed by checking DSP computation time for applying the algorithm of predictive current control and PI-PWM control methods. In this table, we can check that the computation time required by the PDCC method is higher than all other methods due to the higher computational algorithm. But it gives the best performance in terms of current and torque harmonics reduction. The switching frequency for all the methods is shown in the Table. 5, which gives near about the same switching frequency for all the methods. In all the algorithms, free time available is considerable and can include more complex cost functions for a variety of constraints.

C. TORQUE SPEED CHARACTERISTICS

In Fig. 20 torque-speed characteristics are plotted for all the control methods with rated speed and rated torque. Predictive control maintains constant torque up to the 85% of the rated speed while conventional control is unable to maintain the rated torque after 67% of the rated speed. The deadbeat predictive current control (PDCC) shows the best torque-speed curve maintaining average torque up to 87% of the rated speed with minimum torque ripple.

V. CONCLUSION

Predictive current control techniques have been evaluated and implemented on PM BLDC motor for accurately tracking ideal hexagonal trajectory in the stationary plane. The evaluated predictive current control techniques are compared with conventional control technique to verify the performance, and it shows better performance than conventional current control technique for reducing commutation torque harmonic as well as tracking the ideal current, and they are easy to understand and implement.

PI-PWM control fails to maintain average torque after 67% of the rated speed, whereas predictive deadbeat current control works excellent during low-speed and high-speed operation in the same switching frequency operation reducing commutation torque harmonic and accurately tracking ideal hexagonal current trajectory keeping average torque up to 87% of rated speed. The application of commutation and non-commutation vectors in PM BLDC motor operation gives flexibility for operation in three phases and two phases for control during commutation and non-commutation duration, respectively, without increasing computational burden on the processor. The conventional control unable to achieve rated torque at high-speed operation, but predictive control works excellent and achieves rated torque at high speed.

REFERENCES

[1] C. Xia, T. Shi, W. Chen, and Y. Xiao, "Three effective vectors-based current control scheme for four-switch three-phase trapezoidal brushless DC motor," *IET Electr. Power Appl.*, vol. 7, no. 7, pp. 566–574, Aug. 2013, doi: 10.1049/iet-epa.2013.0030.

[2] R. L. Valle, P. M. de Almeida, A. A. Ferreira, and P. G. Barbosa, "Unipolar PWM predictive current-mode control of a variable-speed low inductance BLDC motor drive," *IET Electric Power Appl.*, vol. 11, no. 5, pp. 688–696, May 2017, doi: 10.1049/iet-epa.2016.0421.

[3] J. Park, Y. Kwak, J.-W. Ahn, and D.-H. Lee, "A novel predicted current control scheme of BLDCMs for commutation torque ripple reduction," in *Proc. 18th Int. Conf. Electr. Mach. Syst. (ICEMS)*, Pattaya, Thailand, Oct. 2015, pp. 1429–1433, doi: 10.1109/ICEMS.2015.7385263.

[4] J. Park, Y. Kwak, Y. Jo, J. Bae, and D.-H. Lee, "Torque ripple reduction of BLDC motor using predicted current control," in *Proc. IEEE Transp. Electrific. Conf. Expo, Asia–Pacific (ITEC)*, Busan, South Korea, Jun. 2016, pp. 407–411, doi: 10.1109/ITEC-AP.2016.7512987.

[5] P. Pillay and R. Krishnan, "Modeling, simulation, and analysis of permanent-magnet motor drives. II. the brushless DC motor drive," *IEEE Trans. Ind. Appl.*, vol. 25, no. 2, pp. 274–279, Mar./Apr. 1989, doi: 10.1109/28.25542.

[6] R. Carlson, M. Lajoie-Mazenc, and J. C. D. S. Fagundes, "Analysis of torque ripple due to phase commutation in brushless DC machines," *IEEE Trans. Ind. Appl.*, vol. 28, no. 3, pp. 632–638, May 1992, doi: 10.1109/28.137450.

[7] M. Bertoluzzo, G. Buja, R. Kumar Keshri, and R. Menis, "Analytical study of torque vs. Speed characteristics of PM brushless DC drives," in *Proc. 38th Annu. Conf. IEEE Ind. Electron. Soc.*, Montreal, QC, Canada Oct. 2012, pp. 1684–1689, doi: 10.1109/IECON.2012.6388722.

[8] J.-H. Song and I. Choy, "Commutation torque ripple reduction in brushless DC motor drives using a single DC current sensor," *IEEE Trans. Power Electron.*, vol. 19, no. 2, pp. 312–319, Mar. 2004, doi: 10.1109/TPEL.2003.823177.

[9] W. A. Salah, D. Ishak, B. A. Zneid, A. Abu_Al_Aish, M. S. Jadin, and A. Abu Sneineh, "Implementation of PWM control strategy for torque ripples reduction in brushless DC motors," *Electr. Eng.*, vol. 97, no. 3, pp. 239–250, Feb. 2015, doi: 10.1007/s00202-014-0329-7.

[10] Y.-K. Lin and Y.-S. Lai, "Pulsewidth modulation technique for BLDCM drives to reduce commutation torque ripple without calculation of commutation time," *IEEE Trans. Ind. Appl.*, vol. 47, no. 4, pp. 1786–1793, Jul./Aug. 2011, doi: 10.1109/TIA.2011.2155612.

[11] J. Shi and T.-C. Li, "New method to eliminate commutation torque ripple of brushless DC motor with minimum commutation time," *IEEE Trans. Ind. Electron.*, vol. 60, no. 6, pp. 2139–2146, Jun. 2013, doi: 10.1109/TIE.2012.2191756.

[12] P. Cortes, M. P. Kazmierkowski, R. M. Kennel, D. E. Quevedo, and J. Rodriguez, "Predictive control in power electronics and drives," *IEEE Trans. Ind. Electron.*, vol. 55, no. 12, pp. 4312–4324, Dec. 2008, doi: 10.1109/TIE.2008.2007480.

[13] W. Jiang, Y. Liao, J. Wang, P. Wang, and Y. Xie, "Improved control of BLDCM considering commutation torque ripple and commutation time in full speed range," *IEEE Trans. Power Electron.*, vol. 33, no. 5, pp. 4249–4260, May 2018, doi: 10.1109/TPEL.2017.2717484.

[14] A. G. Castro, W. C. A. Pereira, C. M. R. Oliveira, T. E. P. Almeida, P. R. U. Guazzelli, J. R. B. A. Monteiro, and A. A. Oliveira Junior, "Finite control-set predictive power control of BLDC drive for torque ripple reduction," *IEEE Latin Amer. Trans.*, vol. 16, no. 4, pp. 1128–1135, Apr. 2018, doi: 10.1109/TLA.2018.8362147.

[15] C. Xia, Y. Wang, and T. Shi, "Implementation of finite-state model predictive control for commutation torque ripple minimization of permanent-magnet brushless DC motor," *IEEE Trans. Ind. Electron.*, vol. 60, no. 3, pp. 896–905, Mar. 2013, doi: 10.1109/TIE.2012.2189536.

[16] A. Darba, F. De Belie, P. D'haese, and J. A. Melkebeek, "Improved dynamic behavior in BLDC drives using model predictive speed and current control," *IEEE Trans. Ind. Electron.*, vol. 63, no. 2, pp. 728–740, Feb. 2016, doi: 10.1109/TIE.2015.2477262.

[17] K.-S. Low, K.-Y. Chiun, and K.-V. Ling, "Evaluating generalized predictive control for a brushless DC drive," *IEEE Trans. Power Electron.*, vol. 13, no. 6, pp. 1191–1198, Nov. 1998, doi: 10.1109/63.728346.

[18] G. Buja, R. Menis, and R. Keshri, "Vector analysis of the current commutation in PM BLDC drives," *Bull. Polish Acad. Sci., Tech. Sci.*, vol. 61, no. 4, pp. 829–836, Dec. 2013, doi: 10.2478/bpasts-2013-0089.

[19] W. Jiang, H. Huang, J. Wang, Y. Gao, and L. Wang, "Commutation analysis of brushless DC motor and reducing commutation torque ripple in the two-phase stationary frame," *IEEE Trans. Power Electron.*, vol. 32, no. 6, pp. 4675–4682, Jun. 2017, doi: 10.1109/TPEL.2016.2604422.

[20] W. Jiang, P. Wang, Y. Ni, J. Wang, L. Wang, and Y. Liao, "Multimode current hysteresis control for brushless DC motor in motor and generator state with commutation torque ripple reduction," *IEEE Trans. Ind. Electron.*, vol. 65, no. 4, pp. 2975–2985, Apr. 2018, doi: 10.1109/TIE.2017.2752126.

[21] C. Xia, H. Chen, X. Li, and T. Shi, "Direct self-control strategy for brushless DC motor with reduced torque ripple," *IET Electr. Power Appl.*, vol. 12, no. 3, pp. 398–404, Mar. 2018, doi: 10.1049/iet-epa.2017.0444.

[22] A. G. de Castro, W. C. A. Pereira, T. E. P. de Almeida, C. M. R. de Oliveira, J. Roberto Boffino de Almeida Monteiro, and A. A. de Oliveira, "Improved finite control-set model-based direct power control of BLDC motor with reduced torque ripple," *IEEE Trans. Ind. Appl.*, vol. 54, no. 5, pp. 4476–4484, Sep. 2018, doi: 10.1109/TIA.2018.2835394.

[23] A. D. Alexandrou, N. Adamopoulos, and A. Kladas, "Development of a constant switching frequency deadbeat predictive control technique for field-oriented synchronous permanent-magnet motor drive," *IEEE Trans. Ind. Electron.*, vol. 63, no. 8, pp. 5167–5175, Aug. 2016, doi: 10.1109/TIE.2016.2559419.

[24] M. Tang, A. Gaeta, A. Formentini, K. Ohyama, P. Zanchetta, and G. Asher, "Enhanced DBCC for high-speed permanent magnet synchronous motor drives," *IET Power Electron.*, vol. 9, no. 15, pp. 2880–2890, Dec. 2016, doi: 10.1049/iet-pel.2015.0232.

[25] T. Turker, U. Buyukkeles, and A. F. Bakan, "A robust predictive current controller for PMSM drives," *IEEE Trans. Ind. Electron.*, vol. 63, no. 6, pp. 3906–3914, Jun. 2016, doi: 10.1109/TIE.2016.2521338.

[26] M. P. Kazmierkowski and L. Malesani, "Current control techniques for three-phase voltage-source PWM converters: A survey," *IEEE Trans. Ind. Electron.*, vol. 45, no. 5, pp. 691–703, Oct. 1998, doi: 10.1109/41.720325.

[27] P. Eichenberger and M. Junger, "Predictive vector control of the stator voltages for an induction machine drive with current source inverter," in *Proc. IEEE PESC*, Saint Louis, MO, USA, 2015, pp. 1295–1301, doi: 10.1109/PESC.1997.616936.

[28] A. J. Sonawane, S. P. Gawande, M. R. Ramteke, and S. G. Kadwane, "Nearly constant switching frequency hysteresis-based predictive control for distributed static compensator applications," *IET Power Electron.*, vol. 9, no. 11, pp. 2174–2185, Sep. 2016, doi: 10.1049/iet-pel.2015.0991.

[29] J. Rodriguez, J. Pontt, C. A. Silva, P. Correa, P. Lezana, P. Cortes, and U. Ammann, "Predictive current control of a voltage source inverter," *IEEE Trans. Ind. Electron.*, vol. 54, no. 1, pp. 495–503, Feb. 2007, doi: 10.1109/TIE.2006.888802.

[30] S. Kouro, P. Cortes, R. Vargas, U. Ammann, and J. Rodriguez, "Model predictive control-a simple and powerful method to control power converters," *IEEE Trans. Ind. Electron.*, vol. 56, no. 6, pp. 1826–1838, Jun. 2009, doi: 10.1109/TIE.2008.2008349.

[31] M. Tomlinson, H. D. T. Mouton, R. Kennel, and P. Stolze, "A fixed switching frequency scheme for finite-control-set model predictive control-concept and algorithm," *IEEE Trans. Ind. Electron.*, vol. 63, no. 12, pp. 7662–7670, Dec. 2016, doi: 10.1109/TIE.2016.2593997.

[32] S. Vazquez, J. Rodriguez, M. Rivera, L. G. Franquelo, and M. Norambuena, "Model predictive control for power converters and drives: Advances and trends," *IEEE Trans. Ind. Electron.*, vol. 64, no. 2, pp. 935–947, Feb. 2017, doi: 10.1109/TIE.2016.2625238.

[33] B. Fan, J. Peng, J. Duan, Q. Yang, and W. Liu, "Distributed control of multiple-bus microgrid with paralleled distributed generators," *IEEE/CAA J. Automatica Sinica*, vol. 6, no. 3, pp. 676–684, May 2019.

[34] H. Abu-Rub, A. Iqbal, and J. Guzinski, *High Performance Control of AC Drives With MATLAB/Simulink Models*. Hoboken, NJ, USA: Wiley, 2012.

MANISH S. TRIVEDI was born in Nagpur, India, in 1991. He received the Electrical Engineering degree and the master's degree in power electronics and drives from the Ramdeobaba College of Engineering and Management, Nagpur University, Nagpur, India, in 2013 and 2015, respectively. He is currently pursuing the Ph.D. degree with the Visvesvaraya National Institute of Technology, Nagpur, with a focus on predictive control of permanent-magnet brushless dc motor drive for light electric vehicle. His research interests include predictive control, permanent-magnet brushless dc motor, current control, and space vector control.

RITESH KUMAR KESHRI received the B.Sc. (Engg.) and M.Tech. degrees in electrical engineering from the National Institute of Technology, Jamshedpur, India, in 2003 and 2007, respectively, and the Ph.D. degree in energy engineering from the Department of Industrial Engineering, University of Padova, Italy, in March 2014. Since August 2015, he has been with the Department of Electrical Engineering, Visvesvaraya National Institute of Technology, Nagpur, as an Assistant Professor. His research interests include power electronics and electric drives for electric vehicle propulsion, and charging infrastructure. He received the Silver Medal for being first in the M.Tech. (electrical) degree, in 2007, the Young Researcher Fellowship from the Ministry of University of Italy, in 2008, the Erasmus Mundus Fellowship, for 34 months, from the European Union, in 2010, the First Prize as a Student Team Leader of the University of Padova in class-3 of Formula Electric and Hybrid in 2011, and the 2016 Best Paper Award of the IEEE TRANSACTIONS ON INDUSTRIAL Electronics. He is associated with IEEE-IES and PELS and the Chair for technical track and special sessions in IECON 2013–2019. He is the Chair of the Technical Committee on Transportation Electrification, IEEE Industrial Electronics Society.